

THESIS FOR THE DEGREE OF LICENTIATE OF ENGINEERING

# Multiscale X-ray Characterisation of Cellulose-based Solid Dispersions

MARTINA OLSSON

Department of Physics

CHALMERS UNIVERSITY OF TECHNOLOGY

Gothenburg, Sweden 2022

Multiscale X-ray Characterisation of Cellulose-based Solid Dispersions  
MARTINA OLSSON

© MARTINA OLSSON, 2022.

Department of Physics  
Chalmers University of Technology  
SE-412 96 Gothenburg  
Sweden  
Telephone + 46 (0)31-772 1000

Printed by Chalmers Reproservice  
Gothenburg, Sweden 2022

Martina Olsson  
Department of Physics  
Chalmers University of Technology

## Abstract

Cellulose-based solid dispersions are a promising formulation strategy for providing controlled drug release and dissolution enhancement of poorly soluble drugs. These dispersions can form structures on multiple length scales which can have both positive and negative effects on the functional properties of the formulation. For instance, phase separated morphologies can affect the solubility and release profile of a drug dispersion. Such structures can form both during the processing step or evolve during storage and dissolution. For the development of new pharmaceutical dosage forms and drug delivery systems it is important to develop a better understanding of how these structures are formed and how they will affect the properties of the dispersion. A first step towards establishing this is to develop methodologies for structural characterisation over multiple length scales.

This thesis explores the use of X-ray analysis methods to reveal relationships between structures and morphologies of cellulose-based dispersions to the processing conditions and functional properties of the formulation. The focus is to develop methodologies for multiscale structural characterisation that address the challenges of the inherently low contrast between phases of similar densities and the high sensitivity for radiation damage. In this thesis I show how scanning small and wide-angle X-ray scattering (SAXS and WAXS), ptychographic X-ray computed nanotomography (PXCT) and scanning transmission X-ray microscopy (STXM) can be applied and combined to evaluate multiscale morphologies. First, a partly crystalline solid dispersion of carbamazepine dispersed in ethyl cellulose is imaged with scanning SAXS and WAXS as well as PXCT to develop a workflow for multiscale imaging of solid dispersions. This demonstrates how the nanostructure and type of polymorph can be mapped over a macroscopic sample and image the interior structure of the dispersion with a resolution of 80 nm over an extended sample volume. Secondly, phase separated polymer blends of PLA and HPMC, intended as a polymeric carrier for controlled drug release, are imaged with PXCT and STXM. This reveals the drug distribution as well as the morphology of the two polymer phases, which is related to the dissolution profile of the dispersions, showing a release rate dependent on the morphology of the compound. Finally, the molecular arrangement in melt pressed films is investigated with WAXS to explore changes from water exposure of modified cellulose and relate it to the substituted side chains in the cellulose derivative.

**Keywords:** cellulose, X-ray imaging, multiscale characterisation, solid dispersions, radiation damage, pharmaceutical formulations, SAXS, WAXS, PXCT, STXM.

# List of Papers

This thesis is based on the work contained in the following papers:

- I** Multiscale X-ray imaging of pharmaceutical dosage forms  
**M. Olsson**, R. Govender, A. Diaz, M. Holler, A. Menzel, M. Sadd, S. Abrahamsen Alami, A. Liljeblad, A. Larsson, A. Matic, M. Liebi.  
*Manuscript*
- II** Morphological analysis of phase separated polymer blends in amorphous solid dispersions for controlled drug release  
**M. Olsson**, R. Nilsson, L. Björn, L. Krupnik, P. Naidjonoka, Y. Chen, J. Avaro, A. Diaz, M. Holler, B. Watts, A. Ziolkowska, A. Larsson, M. Liebi, A. Matic.  
*Manuscript*
- III** Screening of hydrogen bonds in modified cellulose acetates with alkyl chain substitutions  
R. Nilsson, **M. Olsson**, G. Westman, A. Matic, A. Larsson  
*Carbohydrate Polymers* 285 (2022): 119188.

## Contribution Report

- I** I planned the PXCT and scanning SAXS and WAXS experiments that was performed together with co-authors. I did the sample preparation for the synchrotron experiments and performed all data analysis. I performed the complementary DSC and wrote the first draft of the manuscript.
- II** I planned the PXCT and STXM measurements that was performed together with co-authors. I performed the sample preparation for the PXCT and performed DSC, WAXS and participated in the dissolution experiments. I performed all data analysis except for the dissolution experiments. I wrote the first draft of the manuscript.
- III** I performed the WAXS measurements and analysis together with co-authors and contributed to the discussion of the results and in writing the paper.

## List of Papers not included in the thesis

- I** Enabling modular dosage form concepts for individualized multidrug therapy: Expanding the design window for poorly water-soluble drugs  
R. Govender, S. Abrahmsén-Alami, S. Folestad, **M. Olsson**, A. Larsson  
*International Journal of Pharmaceutics* 602 (2021): 120625
- II** Experimental Quantum Chemistry: A Hammett-inspired Fingerprinting of Substituent Effects  
F. Sessa, **M. Olsson**, F. Söderberg, F. Wang, M. Rahm  
*ChemPhysChem* 22.6 (2021): 569-576
- III** Cellulose nanocrystals (CNCs) as binding and exfoliating agents for developing flexible composite films as an electrode with MoS<sub>2</sub> nanosheets  
A. Kumar Sonker, S. Xiong, R. Aggarwal, **M. Olsson**, A. Spule, S. Hosseini, S. Kumar Sonkar, A. Matic, G. Westman  
*Preprint available at SSRN doi.org/10.2139/ssrn.4116071*

# Table of Contents

<i>Abstract</i> .....	III
<i>List of Papers</i> .....	IV
<i>Contribution Report</i> .....	V
<i>List of Papers not included in the thesis</i> .....	VI
<i>Table of Contents</i> .....	VII
<b>Chapter 1 - Introduction</b> .....	<b>1</b>
<b>Chapter 2 – Cellulose-based dispersions</b> .....	<b>3</b>
<b>Chapter 3 - X-ray analysis methods</b> .....	<b>7</b>
3.2. Scanning SAXS and WAXS.....	7
3.3. Ptychographic X-ray computed tomography.....	10
3.4. Scanning Transmission X-ray microscopy.....	13
3.4. Radiation damage.....	15
<b>Chapter 4 - Results and Discussion</b> .....	<b>17</b>
4.1. A methodology for multiscale X-ray imaging.....	17
4.2. Relations between morphology, material properties and processing conditions.....	20
4.2.1 Structure formation in extrusion processing.....	20
4.2.2 Morphologies relation to composition and release rate in phase separated dispersions.....	21
4.2.3 Relations between properties and molecular structure.....	24
4.3. Addressing radiation damage.....	25
<b>Chapter 5 - Conclusions and Outlook</b> .....	<b>29</b>
<b>Acknowledgements</b> .....	<b>31</b>
<b>Bibliography</b> .....	<b>33</b>



# Chapter 1 - Introduction

Cellulose is the most abundant biopolymer on earth and present a sustainable option to synthetic polymers as it can be derived from renewable sources, such as wood, cotton or agricultural waste<sup>1, 2</sup>. Another advantage is the large versatility of modified cellulose, providing enormous opportunities to tune e.g., the hydrophobicity and mechanical and thermal properties of cellulose derivatives<sup>3, 4</sup>. Therefore, cellulose derivatives have proven useful in a large variety of applications such as coatings, laminates, additives in building materials, food and for pharmaceutical development<sup>4, 5</sup>. This thesis focusses on cellulose-based solid dispersions for pharmaceutical applications. Solid dispersions describe formulations where a drug is finely dispersed in a polymeric carrier. Dependent on the properties of the carrier, these formulations can provide both extended drug release<sup>6, 7</sup> and increase dissolution of poorly soluble drugs<sup>8</sup>.

The structure and morphology of a solid dispersion will depend on the physical properties of the drug and polymer and the processing conditions, which combined dictate the properties of the final formulation. Amorphous solid dispersions are one example, where a drug is dispersed in its amorphous form in a stabilizing polymeric carrier to improve its solubility<sup>9-12</sup>. Here, the level of mixing between the drug and the polymer is critical to hinder phase transformation or recrystallization causing poor performance<sup>8</sup>. A better understanding of the formation of structures in solid dispersions and how it relates to the properties of the final formulation is therefore of high importance for the development of new solid dosage forms and for new drug delivery systems. Both the solid-state phase, distribution and particle size of the drug will impact physical stability and the release rate of the solid dispersion. To control these properties in the dispersion the impact of process and storage conditions need to be understood as it can induce phase separation or recrystallisation which can fundamentally change the stability and dissolution characteristics. A first step towards this is to develop methodologies for characterising structures over multiple length scales in the dispersions to provide insight to how they relate to processing and storage conditions as well as the properties of the formulation.

X-rays present a versatile toolbox for investigating structures over broad length scales. Two key benefits of using X-rays are the short wavelength (0.1-10Å) and the high penetration power which makes it possible to non-destructively characterise the interior structures of a compound with high resolution<sup>13</sup>. With the advances of high-intensity X-ray techniques provided by synchrotron sources, imaging at multiple length scales is possible with different contrast mechanisms based on e.g., absorption, phase or fluorescence<sup>13</sup>. However, these methods often use high doses of ionizing radiation, making it challenging to apply to radiation sensitive materials such as polymers or biological samples. Often these samples also have low variations in density, making it challenging to obtain contrast based on X-ray absorption. To be able to utilize the wide variety of X-ray techniques for cellulose-based dispersions, these issues need to be addressed.

This thesis investigates the relationship between structure and morphology of cellulose-based solid dispersions to its properties, storage conditions and processing methods. For that purpose, a combination of scanning small- and wide-angle X-ray scattering (SAXS and WAXS), Ptychographic X-ray computed nanotomography (PXCT) and scanning transmission X-ray microscopy (STXM) is applied. The focus is to develop methodologies and workflows for multiscale structural characterisation that address issues of inherently low contrast and radiation sensitivity in cellulose-based dispersions. With the combination of X-ray techniques applied in this thesis different contrast mechanisms and multiple length scales are bridged to gain a deeper understanding of the structure-property-relationships in cellulose-based solid dispersions.

## Chapter 2 – Cellulose-based dispersions

Poor aqueous solubility and slow dissolution rate of drugs are an increasing problem in pharmaceutical development due to a high fraction of poorly soluble substances among new drug candidates<sup>14-16</sup>. Solid dispersions are currently considered one of the most effective methods to improve dissolution and apparent solubility of drug components by formulating bioavailable and therapeutic effective compounds for oral administration<sup>8, 17, 18</sup>. The term solid dispersion is defined as a formulation where one or multiple drugs are dispersed in a carrier matrix. The drug can be molecularly dispersed or dispersed as amorphous or crystalline particles, as illustrated in Figure 2.1, and the carrier can be both amorphous and crystalline<sup>19</sup>. In many cases the drug exists in more than one state in the dispersion.

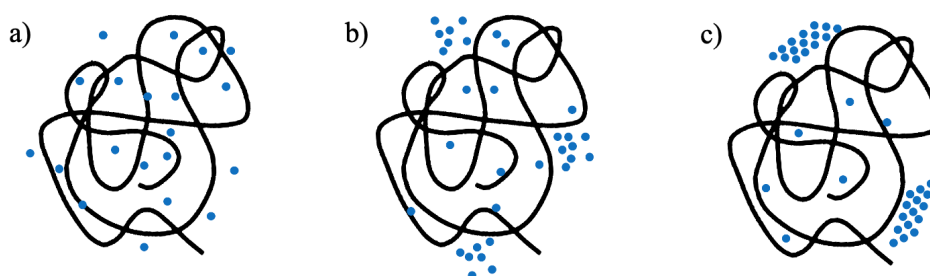


**Figure 2.1.** Solid dispersions of drug molecules (blue) in polymer carrier (black) with the drug a) molecularly dispersed, b) in amorphous aggregates c) in crystalline aggregates.

Solid dispersions can increase the solubility and dissolution rate of poorly water-soluble drugs by reducing drug particle size, enhancing wettability or by changing the crystal phase of the drug to a less stable polymorph, or preferably to the amorphous state<sup>19</sup>. The crystalline form of a drug has the advantage of high physical and chemical stability, but the lattice energy barrier is a major constraint in the dissolution process<sup>16</sup>. The amorphous state, with its disorder structure, has a higher free energy leading to higher apparent water solubility, dissolution rate and oral absorption<sup>20</sup>. However, due to the higher free energy, there is a thermodynamical driving force towards recrystallisation, and the amorphous state needs to be stabilized which can be achieved in a solid dispersion.

This thesis focusses on cellulose-based solid dispersions where the carrier matrix is composed of one or more polymers. Polymers can act as stabilizers to the polymorph of the drug in the solid dispersion due to their complex structures with numerous interchain and intrachain interactions where a dispersed drug can be stabilized by the polymer network due to the reduce molecular mobility<sup>8</sup>. Many properties of solid dispersions can influence the stability, such as an increased glass transition temperature creating a kinetic barrier towards crystallisation, intermolecular interactions between the drug and polymer, e.g. hydrogen bonding, and hygroscopicity of the carrier as absorbed humidity can act as a plasticiser, reducing the stabilizing effect from the polymer carrier on the drug<sup>8</sup>.

Cellulose is a natural polymer which is extensively used in pharmaceutical industry due to the versatility of properties enabled by different modifications<sup>21</sup>, Fig 2.2. By substituting the hydroxyl groups on the cellulose backbone with different side groups, hydrophilicity and thermal and mechanical properties can be adjusted. Three cellulose derivatives that are widely adapted in pharmaceutical industry are Ethyl cellulose (EC), cellulose acetate (CA) and hydroxypropyl methylcellulose (HPMC). Their molecular structures are depicted in Figure 2.2. and as a consequence of the different substituted side groups the three polymers display fundamentally different material properties. While EC is insoluble in water and often used as a coating agent or stabilizer<sup>22</sup>, CA and HPMC are hydrophilic and HPMC is often used in dosage forms for extended release due to its swelling properties<sup>23-25</sup>.

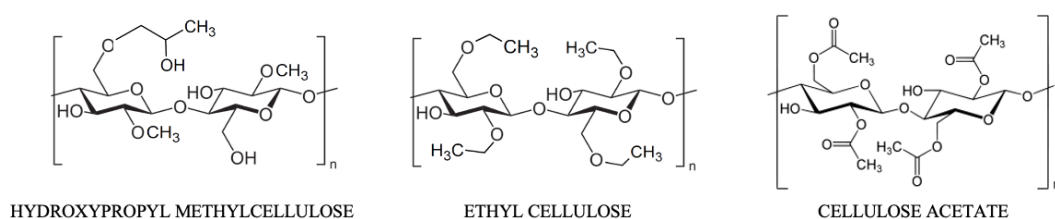


**Figure 2.2.** Chemical structures of the repeating units of HPMC, EC and CA. The substitution of side chains on the cellulose backbone allows for adjustable material properties as exemplified with hydrophilic HPMC and CA in contrast to hydrophobic EC.

Despite the potential and high research interest in solid dispersions the number of marketed products is still low which mainly relates to problems with achieving physicochemical stability during processing and storage, as well as scaling up the manufacturing process<sup>19</sup>. The solid-state of the drug in a solid dispersion is mainly determined by the preparation process and interactions between drug and carrier. During the processing step, phase separation and drug aggregation can occur as well as phase transformations which will affect the structure of the dispersion and the functional properties. Similar events can occur during storage times if the stability is inflicted by moisture absorption or a recrystallisation of amorphous drug domains. To increase the stability of the formulations, it is therefore important to understand the origin of structures formed in solid dispersions and how they will affect the physicochemical properties of the final formulation.

The two main preparation methods for solid dispersions include melting and solvent based methods where hot melt extrusion and spray-drying are the most commonly used due to their high scalability and applicability in pharmaceutical development<sup>26</sup>. In hot melt extrusion, the drug and carrier are simultaneously mixed, heated, melted, and homogenized by being fed into a heated barrel containing one or two rotating screws and finally ejected through a die either in a filament or further injection molded to e.g., pellets and tablets. The intense mixing and agitation from the rotating screws cause disaggregation of drug particles and dispersing in the molten carrier. The advantage of melt processing is that it does not need to incorporate solvents which pose the risk of toxicity and hot melt extrusion is a continuous and efficient technique, easy to scale up which enables industrial application<sup>27</sup>. However, limitations with melt processing are that it requires that the components are thermally stable and miscible in

the molten state. If the components of the dispersion are thermolabile or if the carrier has a very high melting point, solvent-based methods can be used where the solid dispersion is obtained after evaporation of solvent from a solution with the drug and carrier mixture. The solvent-based methods can be problematic as it can be difficult to find a non-toxic solvent where both the hydrophobic drug and hydrophilic carrier are soluble<sup>19</sup>. The complete removal of solvents is also almost impossible and residues remaining can both cause toxicity but also act as a plasticiser in the system, which increase mobility and reduce the stability of the systems.

Solid dispersions are not only useful for increasing dissolution of poorly soluble drugs but can also be used for extended drug release. For instance, water insoluble and swellable polymers which dissolve slowly can be used to sustain the drug release in the release medium<sup>28</sup>. A controlled release enables an adequate amount of drug to be released for an extended period of time which is beneficial both for decreasing toxic side effects of temporarily high drug concentrations, reducing the dosing frequency and enable more constant prolonged therapeutic effects<sup>19</sup>. A release mechanism can be exemplified for a hydrophilic polymer which rapidly dissolves and absorbs water upon contact with the release media and will form a concentrated carrier layer. If the drug dissolves in this layer and the viscosity is high enough to prevent drug diffusion the limiting step in the dissolution process will be the diffusion of the carrier. However, if the drug is not soluble in this layer, the drug may instead be released intact and the dissolution profile will instead majorly depend on the properties of the drug particles such as polymorphic form, particle size and the drug solubility<sup>17</sup>. In insoluble matrixes, the drug release is limited by diffusion or erosion of the polymer matrix which also allow for longer release periods, which can be used e.g., in implants<sup>29</sup>. Therefor the dissolution characteristics of the formulation will be both dictated by the drug and carrier and the level of dispersion between them.



# Chapter 3 - X-ray analysis methods

X-ray techniques is a versatile toolbox for studying cellulose-based dispersions. X-rays are electromagnetic radiation with a wavelength ranging from 0.01-10 nm, corresponding to energies in the range 100eV to 100keV<sup>13</sup>. X-rays with high energy, above 5-10 keV are called hard X-rays while those with lower energy are called soft X-rays. Soft X-rays are particularly useful in spectroscopy as it allows for studying absorption edges of many elements in the periodic table and can probe the chemistry of the sample based on the local bonding and coordination environment.<sup>30</sup> Hard X-rays are particularly useful for imaging as the short wavelength leads to a low diffraction limit ( $\sim\lambda/2$ ), allowing for imaging with high resolution, and a high penetration depth for soft materials which allows for non-destructive 3D imaging<sup>31</sup>. Most X-ray imaging techniques relies on density differences, which dictates X-ray absorption in the sample for contrast, but also scattering and spectroscopy can be combined with imaging to provide contrast based on a particular scattering signal or chemical information obtained from spectroscopic signatures. In this thesis scanning SAXS/WAXS, PXCT and STXM with NEXAFS contrast are used for imaging structures in cellulose-based solid dispersions.

## 3.1 Scanning SAXS and WAXS

Small- and wide-angle X-ray scattering (SAXS/WAXS) generate structural information on the nano to Ångström length scale, statistically averaged over the volume illuminated by the X-ray beam. Figure 3.1 shows the geometry of a scattering experiment in transmission. The sample is exposed to a monochromatic X-ray beam, defined by the wave vector  $\vec{k}_0$ . When X-rays interact with the sample, it will be partly scattered at an angle,  $2\theta$ , defined by the wave vector  $\vec{k}_s$ . The scattering process is considered elastic, meaning that the energy of the X-ray wave is conserved and that  $|\vec{k}_0| = |\vec{k}_s|$ . The scattering vector,  $\vec{q}$ , is defined by the difference of the two wave vectors and describes the momentum transfer of the scattering process according to

$$q = |\vec{q}| = |\vec{k}_s - \vec{k}_0| = \frac{4\pi}{\lambda} \sin \theta \quad \text{Equation 3.1}$$

where  $\lambda$  is the wavelength of the X-ray beam. The scattering can be translated to an approximate real space distance according to  $q = 2\pi/d$ . Since the investigated length scale is related to the scattering vector, structures of different length scales are probed depending on the investigated q-range. This is determined by the sample-to-detector distance where a shorter distance probes wide scattering angles (WAXS), corresponding to smaller structures, while a longer distance probes smaller scattering angles (SAXS) related to larger structures, Figure 3.1. SAXS usually refer to scattering angles below  $1^\circ$  while WAXS, also called X-ray diffraction (XRD), cover larger angles<sup>32</sup>.

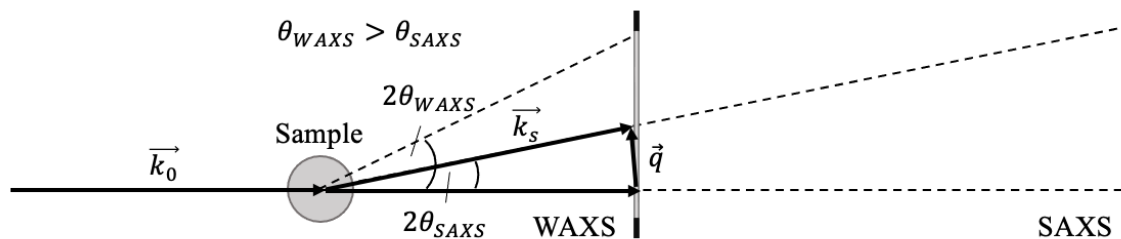


**Figure 3.1.** Schematic of the geometry of a scattering experiment in transmission. The incident X-ray is scattered by the sample with an angle  $2\theta$ . Depending on the sample-to-detector distance different angular ranges are captured where a longer distance capture smaller angles and hence denoted as the SAXS regime.

With using a focused X-ray beam in the scattering experiment, high spatial resolution can be achieved and by raster-scanning the sample over the focused beam, an image can be created where each pixel contains information from the scattering pattern in that specific point. Often a micro focused beam is used, and the beam and step size selected will determine the spatial resolution of the measurement, as each step corresponds to one pixel. The pixel value in the image can either represent the intensity of a feature in the scattering pattern, e.g., the intensity from a crystalline peak but it can also be set by a property derived from the scattering pattern, such as orientation or domain size<sup>33</sup>. A schematic experimental setup for a scanning SAXS/WAXS experiment is shown in Figure 3.2 where the X-ray is focused in a small spot on the sample and the scattering pattern is collected with a two-dimensional detector.

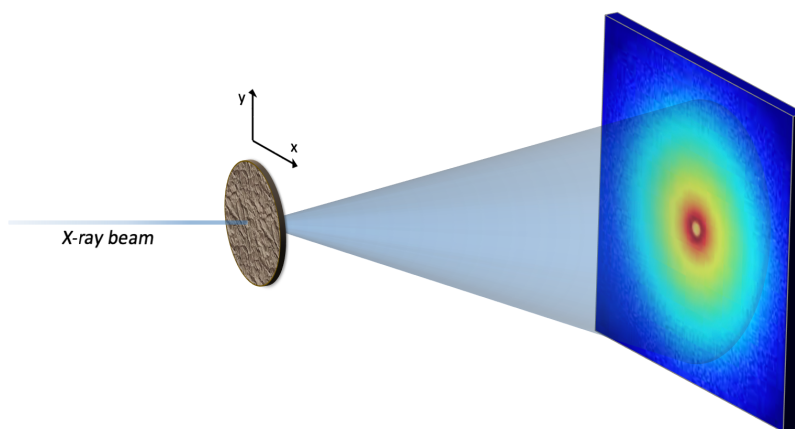


**Figure 3.2.** Schematic setup for scanning SAXS/WAXS. The sample is raster-scanned over a micro focused beam and a 2D scattering pattern is collected in each point.

SAXS and WAXS can be applied to a variety of samples and sample thicknesses. However, there are optimal thicknesses for maximizing the scattering intensities. A too thick sample will lead to high absorption and multiple scattering events which smears the detected signal while a too thin sample can lead to very few scattering events and consequently, a low signal-to-noise ratio<sup>34</sup>. An optimal sample thickness has been derived to have a transmission of  $1/e$  which limit multiple scattering events while the statistics are kept high<sup>34,35</sup>. Another aspect to consider for the sample preparation specifically for scanning SAXS/WAXS experiments is the isotropic spatial resolution needed. Since the scattering pattern contains all nano-structural information averaged over the illuminated volume, both beam size and thickness of the

sample will determine the resolution. If the requirements for the resolution along the beam path can be relaxed, then the technique can also be applied to thicker samples such as a full extruded rod or an entire tablet.

Figure 3.3a shows an example of a two-dimensional WAXS pattern of a solid dispersion. The colour indicates the intensity of the signal i.e., the normalised number of photons registered by each pixel in the detector. The scattering data can be analysed by two approaches as demonstrated in papers I, II and III. First, to generate an average scattering curve the scattering pattern is radially integrated over the full azimuthal range, generating a 1D curve as shown in Figure 3.3b. This information is used to resolve nano-structural features of the material, such as average sizes and shapes, by applying different models to fit the scattering curve for SAXS and evaluating scattering peaks for characterising the solid-state and molecular arrangement in WAXS. Secondly, the asymmetry of the scattering can be investigated to extract information about the anisotropy of the material. This analysis can be performed according to the approach proposed by Bunk et al.<sup>33</sup> where the detector is divided into azimuthal segments as illustrated in Figure 3.3a. Figure 3.3c shows the integrated intensity values in a selected q-range for each azimuthal segment (circles). This intensity distribution over the detector can be fitted by a cosine function where the baseline of the cosine function  $a_0$ , gives the symmetric intensity in the specific q-range, averaged over all segments. The amplitude  $a_1$ , gives the intensity of the asymmetric scattering which corresponds to the oriented part of the scattering. The peak position, or the phase of the cosine function,  $\phi_s$ , corresponds to the scattering angle of orientation and the ratio between  $a_1/a_0$  can be defined as the degree of orientation in the sample.

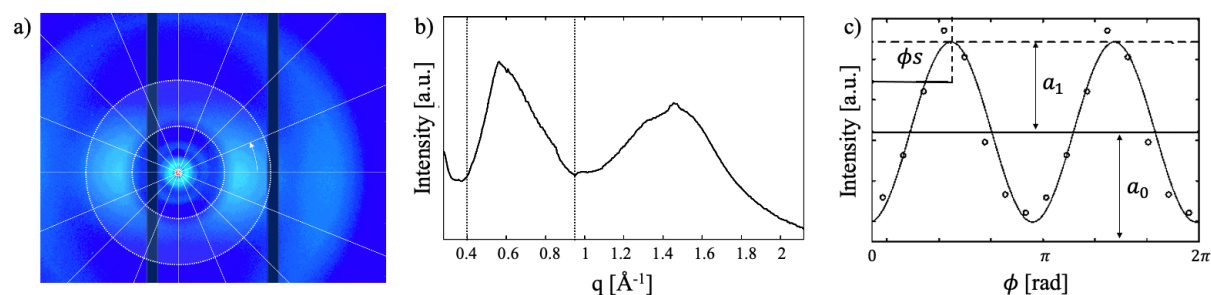


**Figure 3.3.** WAXS data from an extruded ethyl cellulose-based dispersion a) 2D pattern divided in 16 azimuthal segments b) radially integrated intensity of the full q-range over all azimuthal segments in the 2D detector and c) integrated intensity values in the indicated q range for each segment with the dashed lines in the 2D detector and integrated curve. The azimuthally integrated values are fitted with a cosines curve to extract angle of orientation,  $\phi_s$  and degree of orientation,  $a_1/a_0$ .

The WAXS measurements in paper II were performed directly through the full extruded filament using a lab scale Mat: Nordic X-ray scattering instrument (SAXSLAB) equipped with a high brilliance Rigaku 003 X-ray micro-focus, Cu-K $\alpha$  radiation source ( $\lambda = 1.5406 \text{ \AA}$ ) and a Pilatus 300 K detector. The exposure time was 300 s and the sample-to-detector distance 134 mm. The WAXS measurements in paper III were performed on cellulose derivatives as melt pressed films unconditioned and conditioned by being soaked in water 72 h prior to the measurement using the same lab scale instrument. The wet films were carefully wiped clean

from excessive water adsorbed on the surface of the films and mounted in sandwich cells with Kapton windows to keep the set condition during the measurements. An exposure time of 300 s and a sample-to-detector distance of 134 mm was applied. The background signal from Kapton was subtracted prior to analysis.

The scanning SAXS and WAXS measurements in paper I was performed at the cSAXS beamline (X12SA) at the Swiss Light Source, Paul Scherrer Institute (Switzerland). The energy was set to 11.2 keV and the beam size to  $25 \times 25 \mu\text{m}^2$ . A He-filled flight tube was placed between the sample and detectors to reduce air scattering. A Pilatus 2M detector was placed 7m downstream of the sample to measure SAXS and a Pilatus 300k oriented as a vertical strip was placed below the sample to simultaneously measure WAXS. The extruded filament was measured both perpendicular to the extrusion direction, over the intact filament, and in the direction parallel to the direction of extrusion through a cut cross section of the filament. The section was cut to a thickness of  $25 \mu\text{m}$  to match the beam size and get an isotropic resolution. A step size of  $25 \mu\text{m}$  and an exposure time of 0.1s was applied. The two-dimensional scattering patterns were radially integrated to retrieve one-dimensional scattering curves with the *cSAXS scanning SAXS package* developed by the CXS group, Paul Scherrer Institute, Switzerland.

### 3.2 Ptychographic X-ray computed tomography

Ptychographic X-ray computed tomography (PXCT) is a quantitative, high resolution imaging technique that combines the phase reconstruction method of ptychography with tomographic imaging and quantitatively resolves the electron density distribution in three-dimensions<sup>36</sup>. Tomography is a non-invasive 3D imaging technique where projections of the sample are measured from multiple angles<sup>37</sup>. A projection measures the accumulated X-ray interaction along the thickness of the sample. Mathematically, this is equivalent of taking the line integral of the X-ray interaction along the total path of the X-ray beam for each vertical slice of the object. These line integrals, collected at many rotation angles of the sample, can then be reconstructed to reproduce the interior 3D volume of the sample. For this, various reconstruction algorithms exist where the most common applied is filtered back projection<sup>38</sup>.

Standard tomography relies on the absorption contrast of samples, which is measured by the attenuation of the beam as it interacts with the sample<sup>37</sup>. However, as X-rays pass through a sample, it will inflict both an attenuation and phase shift to the incident beam. This is defined by the complex refractive index,  $n(\mathbf{r})$ , which describes the response of electrons to the electromagnetic radiation expressed as

$$n(\mathbf{r}) = 1 - \delta(\mathbf{r}) + i\beta(\mathbf{r}) \quad \text{Equation 3.2}$$

where  $\delta(\mathbf{r})$  is the refractive index and  $\beta(\mathbf{r})$  the absorption index. Both terms depend on the energy of the electromagnetic radiation, with  $\delta(\mathbf{r}) \propto E^{-2}$  and  $\beta(\mathbf{r}) \propto E^{-4}$ <sup>36</sup>. This means that with high X-ray energy, most materials exhibit phase changes that are more pronounced by orders of magnitude compared to absorption variations. This is especially useful for low z elements as encountered in cellulose-based materials due to their low absorption<sup>39</sup>. The reason

for absorption being the more common contrast mechanism in tomography experiments is due to the phase problem which comes from that the phase of the wave is much harder to measure<sup>40</sup>. Normal detectors only measure the intensity of the X-ray beam, and the phase information is lost. To also utilize the phase contrast, phase retrieval methods can be applied in combination with tomography. Ptychography is one example of a phase retrieval method which originates from coherent diffraction imaging<sup>41</sup>.

Ptychography is based on measuring the intensity of the far-field diffraction pattern using a coherent beam<sup>40</sup>. The coherence permits for a retrieval of the phase using iterative algorithms based on constrains in both real and reciprocal space. These constrains require that the diffraction pattern recorded is oversampled which is done by a specific scanning procedure where a micro focused beam is scanned over a sample with an overlap between adjacent illuminated position, which provides a sufficient over-sampling of the object. For the iterative reconstructions, the oversampling gives a real space constraint by the position of the beam and the reciprocal constrain is given by the diffraction patterns collected in each point<sup>40</sup>. The reconstructed phase can then be converted to absolute electron density,  $n_e(\mathbf{r})$ , with a linear relationship as described by Diaz et.al.<sup>42</sup>

$$n_e(\mathbf{r}) = \frac{2\pi\delta(\mathbf{r})}{\lambda^2 r_0} \quad \text{Equation 3.3}$$

where  $r_0$  denotes the classical electron radius,  $\delta(\mathbf{r})$  is the difference from unity of the real part of the refractive index distribution within the object and  $\lambda$  is the wavelength of the radiation. This procedure generates a 2D projection of the phase of the sample which for PXCT can be used as input for tomographic reconstruction to extend the information to 3D and obtain the electron density distribution in the sample volume.

A schematic experimental set up for PXCT is shown in Figure 3.4. A micrometre sized sample (10-100  $\mu\text{m}$ ) placed on a rotation stage is illuminated by a focused beam and a detector is placed in the far-field regime to collect the diffraction pattern in each scan point. In this way, a ptychographic projection is computed for each rotation angle as input for the tomographic reconstruction. Since PXCT is a lensless imaging technique, it overcomes limitations in resolution induced by X-ray optics and the resolution is instead ultimately limited by the angular range of the diffraction pattern that can be collected with sufficient signal-to-noise ratio<sup>43</sup>. However, the achievable resolution is also dependent on the scanning point accuracy, the mechanical stability of the measuring system and the sample composition<sup>43</sup>. For soft materials such as cellulose, radiation damage is often the limiting factor as it dictates the radiation dose that the sample can be exposed to during the measurements.

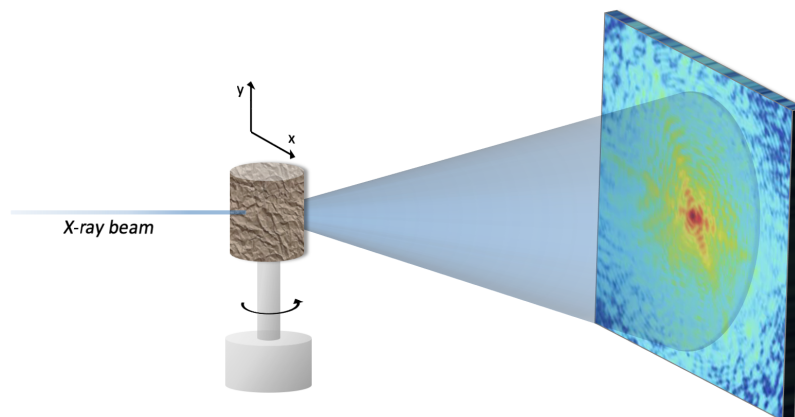


**Figure 3.4.** Schematic setup for PXCT. A micrometre sized sample is placed on a rotational stage and illuminated by a focused coherent beam and the far-field diffraction pattern is collected in each point. The sample is raster-scanned to build up ptychographic projections for each rotation angle which is used for the tomographic reconstruction.

The PXCT measurement requires samples to be prepared with a size in the order of 10 to 100  $\mu\text{m}$  to allow for high resolution and reasonable measurement times ( $\sim$ hours). In Paper I and II this was done by mechanical milling of an extruded samples using a lathe system developed at the cSAXS beamline<sup>44</sup>. The milled sample is prepared in minutes, making it a time- and cost-efficient method compared to e.g., focused-ion-beam milling which is also commonly applied<sup>36, 43, 45</sup>. Mechanical milling is also a good option for radiation sensitive materials where the electron beam poses a risk for damaging the material. Mechanical milling may induce elevated temperatures in the sample which can cause problems for samples with low glass transition and melting temperatures. To hinder this, a setup with a cryogenic chamber filled with liquid nitrogen can applied, cooling both the sample and lathe system.

The PXCT measurements in paper I and II were both performed at the cSAXS beamline (X12SA) at the Swiss Light Source, Paul Scherrer Institute (Switzerland) under cryogenic conditions using the OMNY-setup<sup>46</sup>. The energy was set to 6.2 keV and a Fresnel zone plate was used for focusing a coherent beam onto the specimen with a beam size of  $\sim 4 \mu\text{m}$ . The detector was placed 7.2 m downstream of the sample with a flight-tube in between the OMNY hutch and an Eiger 1.5M detector. Ptychographic scans were made over the full field of view of the cylindrical pillars, including air on each side of the sample, with a step size of  $2 \mu\text{m}$ . At each scanning position diffraction patterns were collected with an acquisition time of 0.025s and 0.05s, respectively. The ptychographic scans were collected at equally spaced angles from  $0^\circ$  to  $180^\circ$  generating 1600 projections for the tomographic reconstruction. The program *Ptychoshelves* was used for ptychographic and tomographic reconstructions<sup>47, 48</sup>. Ptychographic scans were reconstructed using the difference map algorithm described by Thibault et al.<sup>49</sup> and tomographic reconstruction was performed using a filtered back projection algorithm. The resolution was determined to be  $\sim 100 \text{ nm}$  in the dispersions by Fourier shell correlation (FSC)<sup>50</sup>.

### 3.3 Scanning Transmission X-ray microscopy

Scanning transmission X-ray microscopy (STXM) is a high-resolution imaging method where a sample is raster-scanned over the X-ray beam and an image is built up based on the transmission intensity in each point<sup>51</sup>. The spatial resolution of a STXM experiment is typically 30 nm, limited by the focus achieved for the X-ray beam, although for combinations with ptychographic coherent diffraction imaging, a resolution of 10 nm has been reported<sup>52</sup>. Depending on the selected energy, different contrast mechanisms can be used, both in the soft and hard X-ray regime. It can also be coupled with X-ray absorption spectroscopy by changing the energy of the incident beam which result in a combination of imaging with both high spatial and high spectral resolution. A schematic setup for a STXM experiment is shown in Figure 3.5. A monochromatic X-ray beam is focused onto the sample using a Fresnel zone plate and an order sorting aperture (OSA) is used to block the unfocused zero-order beam and higher diffraction orders resulting in a highly focused X-ray beam to reach the sample. After the sample, a detector collects the transmitted X-ray beam.

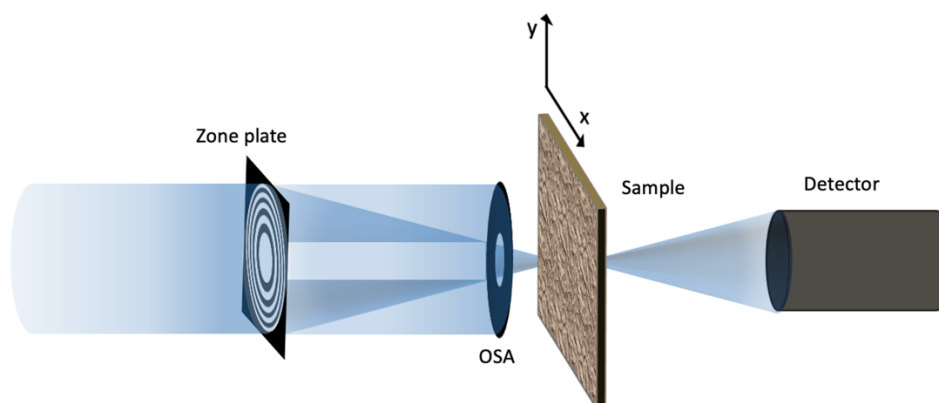


**Figure 3.5.** Schematic setup for a STXM experiment. A monochromatic X-ray beam is focused onto the sample and the transmitted intensity is collected by a detector. To build up an image, the sample is raster-scanned over the beam, generating a transmission value measured in each pixel.

X-ray absorption spectroscopy is used to study absorption edges of elements, i.e. the onset energy for inner-shell ionisation of the specific element<sup>53</sup>. An absorption edge can be found for each inner shell energy level and the concentration of a particular element can be determined quantitatively from the difference in absorption just above and just below the absorption edge<sup>53</sup>. With a high spectral resolution, the fine details of the absorption edge can be resolved to also characterise the chemical structure of the material by studying the near edge X-ray absorption fine structure (NEXAFS)<sup>54</sup>. The features resolved in a NEXAFS spectrum correspond to electronic excited states in which an inner-shell electron is excited to an unfilled molecular orbital or out to the continuum, Figure 3.6a. Since the energy is increasing throughout the absorption edge, the first structures detected are related to excitations to the lowest unoccupied molecular orbital (LUMO) followed by higher energy unoccupied molecular orbitals and the ionization potential. If the investigated material has  $\pi$ -bondings, i.e., double or triple bonds, the LUMO is usually a  $\pi^*$ -orbital while  $\sigma^*$ -orbitals, associated with single bonds, are found at higher energies<sup>53</sup>. Figure 3.6b shows a schematic

NEXAFS spectrum where different resonance energies correspond to different electronic transitions characteristic for the electronic structure of the material. The electronic structure is determined by both the geometric and covalent bonding structure and NEXAFS spectra can differ significantly between rather similar molecules, which can be particularly useful for detecting small molecular difference in e.g., modified cellulose<sup>55</sup>.

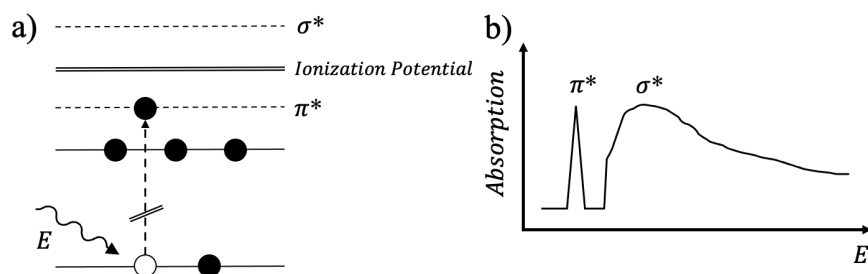


**Figure 3.6.** a) Schematic over electronic transitions between the core level energies and unoccupied molecular orbitals due to X-ray absorption. b) Schematic over a NEXAFS spectra corresponding to the electronic transitions to the unoccupied molecular orbitals illustrated in a).

Since STXM with NEXAFS contrast relies on the detection of the transmitted X-ray signal, the thickness of the sample is important. A too thick sample will lead to no transmitted signal and too thin samples will lead to poor signal due to no significant absorbance. Since cellulose and polymers are carbon-based molecules NEXAFS studies around the carbon K-edge (280-320 eV) are most efficient for evaluating the structure, potentially in combination with the nitrogen and oxygen K-edges. At this energy, the absorption is high and to allow sufficient transmission samples need to be prepared with a thickness of about 100nm. The transmitted signal is often converted to an optical density,  $OD(E)$ , according to

$$OD(E) = \ln(I_0/I) \quad \text{Equation 3.4}$$

where  $I_0$  is the incident X-ray flux for a given energy and  $I$  is the transmitted flux through the sample<sup>56</sup>. An optical density between 1-2 is often appropriate to allow a significant transmission through the sample. The optical density is related to the sample properties by

$$OD(E) = \mu(E)\rho t \quad \text{Equation 3.5}$$

where  $\mu(E)$  is the mass absorption coefficient of the material,  $\rho$ , the density and  $t$  the thickness of the material<sup>56</sup>. This relation also allows for quantitative imaging.

For the STXM measurements in Paper II, the extruded samples were cut in sections with a thickness of 150 nm using an ultramicrotome. The thin sections were mounted on 100 nm thin silicon nitride,  $\text{Si}_3\text{N}_4$ , membrane, which have low absorbance in the specified energy range. The measurements were performed at the PolLux beamline at the Swiss Light Source, Paul Scherrer Institute (Switzerland). The sample chamber was pumped to ultra-high vacuum  $\sim 10^{-6}$  mbar to avoid air absorption. The dispersions were measured by scanning the energy of the carbon K-edge, in the range 280-330 eV with high spectral resolution (0.1 eV), to resolve the NEXAFS spectra of the dispersions. To investigate the morphology and drug

distribution of the dispersions an image was built up by raster scanning the sample with high resolution (30-100 nm) at resonance energies specific for each compound in the dispersion. In that way an energy stack is built up for each pixel containing the optical density at each resonance energy.

### 3.4 Radiation damage

Radiation damage occurs whenever ionizing radiation is absorbed by a material and often cause problems for characterising soft materials, such as cellulose<sup>57</sup>. When X-rays interact with the sample, energy is deposited through inelastic scattering and photoelectric absorption, which is released in a cascade of electrons which can cause reactions leading to breaking of chemical bonds, redox processes and generating free radicals<sup>58</sup>. This can impose structural and chemical alterations to the sample during the measurement and hinder proper characterisation. The radiation damage is therefore related to the number of photons the sample is exposed to, referred as the radiation dose<sup>57</sup>. With typical lab sources, the brilliance is on the order of  $10^9$  photons/s/mm<sup>2</sup>/mrad/0.1%bandwidth while for synchrotron sources  $\sim 10^{20}$  photons/s/mm<sup>2</sup>/mrad/0.1%bandwidth. With the increased brilliance of 4<sup>th</sup> generation synchrotron sources, problems with radiation damage becomes more and more evident<sup>13, 59</sup>. The radiation damage is ultimately determined by the accumulated radiation dose of the sample but depends also on different factors such as the X-ray wavelength and sample environment. However, the mechanism of radiation damage is complicated and a comprehensive understanding of the issues involved is still lacking<sup>60</sup>.

For X-ray imaging the X-ray dose required to image the sample is inversely proportional to the fourth power of the aimed resolution and radiation damage in organic materials are often one of the limitations for the resolution and sensitivity of the measurement<sup>41, 61</sup>. To be able to apply these techniques where high doses are inevitably needed to cellulose-based dispersions the effects of radiation damage need to be minimized. One such strategy is to apply cryogenic sample protection which partially mitigates radiation damage in the sample. Measurements under cryogenic conditions have been shown to be effective in preserving structures and minimizing mass loss, however the damage to chemical bonds have been shown to be similar in cryogenic conditions and room temperature<sup>62</sup> meaning that the sample is still exposed to the radiation damage but the cryogenic conditions contributes with keeping the structure intact during the measurement. Therefore, cryogenic conditions can be more or less effective depending on the chosen contrast mechanism of the technique.

For the techniques discussed in this thesis radiation damage is of high relevance for PXCT and STXM with NEXAFS imaging where a high dose is needed for high-resolution. In scanning SAXS/WAXS this problem is not as severe since the radiation dose can be kept much smaller. PXCT uses hard X-ray energies and is dose-effective thanks to the removal of lenses and each measurement point does not impose a severe radiation dose on the sample. However, to reach a good signal-to-noise ratio for enabling imaging with high resolution and high contrast, many projections are needed, accumulating a high radiation dose during the measurement. STXM with NEXAFS operates with soft X-rays which cause more damage for

cellulose-based materials due to the high absorption cross sections of C, N and O K-shells<sup>60</sup>. Measuring around the absorption edges impose a high X-ray absorption which quickly builds up to a high accumulated dose due to the high fraction of photons that are absorbed from the incident X-ray beam.

# Chapter 4 - Results and Discussion

This thesis explores the use of X-ray imaging and characterisation techniques for evaluating structures and morphologies of cellulose-based dispersions. To do this a variety of X-ray techniques have been applied, including X-ray imaging, scattering and spectroscopy-based methods. X-ray imaging has the advantage of forming an image of structures and morphologies in real space, which simplifies analysis and allow for a direct correlation between observed morphologies to e.g., the processing conditions and properties of the material. X-ray scattering is useful for evaluating a sample at the smallest length scales, by probing the nano-structural and molecular arrangements. By coupling X-ray scattering with a micro-focused beam and scanning stages, it also allows for imaging of the structural information over a large sample size. Spectroscopy based methods utilize the information obtained from X-ray absorption as a function of wavelength and can provide information on chemical and elemental properties. With the combination of different X-ray techniques, complementary information from multiple length scales and contrast mechanisms can provide a deeper understanding of the properties of the dispersion. The results presented in this thesis demonstrate how the different utilized X-ray techniques can complement each other and be adapted for addressing radiation sensitive cellulose-based solid dispersions. For three cellulose-based systems this is exemplified by relating the resolved structural properties to the material properties and processing conditions of the specific compound.

## 4.1 A methodology for multiscale X-ray imaging

Solid dispersions have structures on multiple length scales that are created as a consequence of composition, processing method, storage conditions or form upon contact with the dissolution media. On the smallest length scale, WAXS can be used to study the molecular arrangement and provide information on the solid-state phase of the dispersion, e.g., if the drug is dispersed in amorphous or crystalline form and if there are different polymorphs present in the dispersion. On a slightly larger size scale, SAXS can be used to study the nanostructure of dispersions and reveal inhomogeneities by correlating the scattering pattern to the internal structures. In solid dispersions this can for example reveal nano and microstructures from aggregation of drug particles, microporosity and phase separation. PXCT can be used to image the microstructure in real space, with resolutions below 100 nm, by resolving the 3D morphology of the dispersion<sup>36</sup>. While these techniques provide structural information based on changes in electron densities, STXM provide chemical information derived from the absorption of the sample at resonance energies related to chemical transitions in the material<sup>53</sup>. The resolution is similar to that of PXCT and can be useful for distinguishing between species of similar densities, but with different chemical content. For instance, this can be used for quantifying drug content and distribution of dispersed drug which gives minor increase in electron density but can have clear contrast in STXM due to chemical contrast. The four techniques provide information on different length scales and depends on different interactions with the X-ray beam. By combining these techniques, X-

ray imaging can be performed over multiple length scales, bridging the information gained at the Ångström scale to the macroscopic scale of millimetres in solid dispersions as illustrated in Figure 4.1.

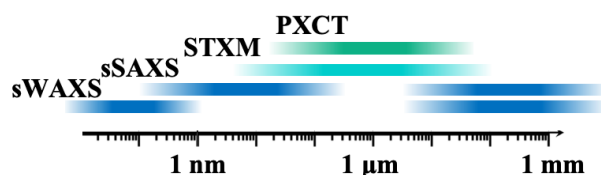


**Figure 4.1.** Length scales probed by PXCT, STXM and scanning SAXS and WAXS. By combining the techniques, X-ray imaging can be performed over multiple length scales as described in paper I and paper II.

The combination of PXCT and scanning SAXS/WAXS is applied in paper I where a methodology is developed for multiscale characterisation of structure and morphology in pharmaceutical formulations. To illustrate the capabilities of this methodology, we imaged a partly crystalline solid dispersion of carbamazepine in ethyl cellulose prepared by melt extrusion. Figure 4.2 illustrates the information obtained from the two techniques. Scanning SAXS/WAXS is performed over the full bulk of the extruded filament as well as over a cross section of the filament with a micro focused beam using a step size of 25  $\mu\text{m}$ . From the scattering pattern in each pixel, the average domain size, orientation and dominating polymorphic form is determined and this is used to construct an image of heterogeneities over the cross section of the extruded filament, Figure 4.2. PXCT is performed on a sub-volume with a diameter of 50  $\mu\text{m}$ , extracted from the centre of the extruded filament. The experiment image the electron density distribution in the sample with a resolution of 80 nm visualizing, the carbamazepine rich domain distribution and shape of carbamazepine crystals in the ethyl cellulose matrix.

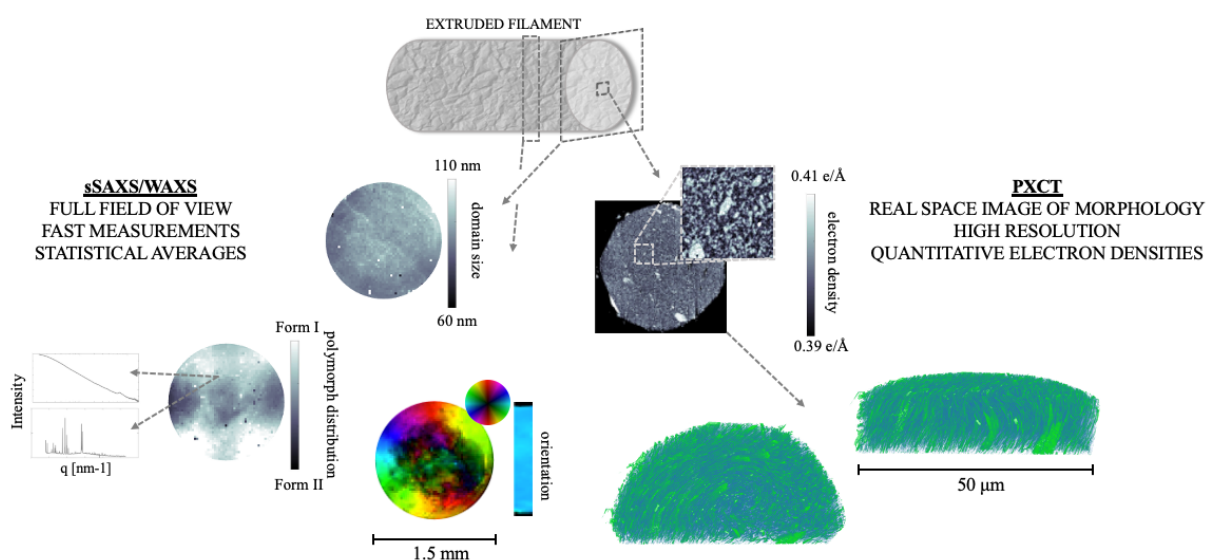


**Figure 4.2.** Overview of results gained from the combined use of scanning SAXS/WAXS and PXCT from paper I.

The selected step size for the scanning SAXS/WAXS measurements (25  $\mu\text{m}$ ) and the size of the sub volume for PXCT (50  $\mu\text{m}$ ) was adapted to provide a sufficient overlap and bridge the length scales probed in the two measurements. Similarly, the detector distance for SAXS was adapted to provide an overlap with the size of the probed nanostructures (1-500 nm) with the resolution of the PXCT measurement (80 nm). This bridging of resolved length scales are beneficial for several purposes. Firstly, the images resolved in PXCT measurement gives a detailed description of the morphology but although a large volume is probed with respect to the high resolution, (d=50  $\mu\text{m}$ , 80 nm resolution ) the 50  $\mu\text{m}$  cylinder is a small subset of the full volume and it needs to be established if this is a morphology that can be expected to be representable for the full volume or if the nanostructure is expected to change over the filament. Here, the statistical approach of scanning SAXS works excellent for comparing if the scattering of the sample is similar over a larger volume, and hence determining if the morphology in the PXCT measurement can be deemed representable for the sample.

Secondly, the nano structural information in a scanning SAXS experiment is derived from the scattering pattern of the sample, which is a representation of the square of the Fourier transform of the electron density distribution, averaged over the illuminated volume. This can be difficult to directly convert to an interpretation of the nanostructure in real space and often requires assumptions to be made. With the direct image of structures resolved in the PXCT measurement, information on the type of structures, e.g., size, shape, and size distribution, can be used as boundary conditions for the scanning SAXS analysis and simplify and improve the interpretation.

Thirdly, PXCT has a remarkable capability of resolving small electron density differences and to determine if a component is amorphous or crystalline is often easily done directly from the electron density values of different phases. However, determining the crystalline polymorph can be trickier, depending on the electron density difference between phases and although it is in theory possible to distinguish crystalline polymorphs from each other, it can be hard to in practice separate them. Uncertainties in the conversion to absolute units can also play a role when evaluating small differences in contrast and here diffraction is a more reliable technique for characterising the crystalline phase. The combination of scanning WAXS works well for correlating what polymorphic form are present in the dispersion, with the addition of also being able to analyse heterogeneities in the distribution of the polymorph over the scanned area of the sample.

These advantageous were applied for the analysis of the dispersion in paper I and it was deemed that the imaged morphology in the PXCT measurement is representable of the entire extruded filament. Another approach for the combined use of the two techniques is to use the scanning SAXS/WAXS measurements to select regions of interest in the sample for where it would be interesting to perform a more detailed study using nanotomography. This is especially useful for samples with high heterogeneity to confirm that the region prepared for PXCT contains the information of interest. In addition, this allows for the SAXS/WAXS and PXCT measurement to be performed on the exact same volume, which enables a direct correlation of the nano and micro-structural information. In addition, the radiation dose

inflicted on the sample in a scanning SAXS/WAXS measurement is neglectable in comparison to the nanotomography and is considered safe to be performed on the sample before the PXCT measurement. However, performing a SAXS/WAXS measurement on the same sample after PXCT is not advised due to the risk of significant radiation damage.

## **4.2 Relations between morphology, material properties and processing conditions**

The structure and morphology, at all length scales, in a material will affect its properties. The formation of structures in solid dispersions are dictated by the composition, storage, and processing conditions. Studying the effect of the morphology on the properties are important both for gaining a deeper understanding of the relationship between processing, morphology, and functionality but also to open for the possibility to tailor properties of future solid dispersion-based compounds by controlling their structures. This is exemplified in paper I, II and III where the structure and morphology of cellulose-based materials are related to their functional properties and processing method. In paper I, we demonstrate how the high shear of the melt extrusion process creates a highly oriented distribution of crystalline carbamazepine domains in an ethyl cellulose-based dispersion. In paper II we show how the composition and resulting viscoelastic properties of the melt mixture in the extrusion process create different phase separated morphologies in a solid dispersion of nicotinamide dispersed in a mixture of PLA and HPMC. The morphologies are also related to the dissolution profile of the dispersions, establishing a connection between the morphology and the dissolution characteristics to enable tailoring of the drug release rate. In paper III we explore how the structure of modified side chain groups on the polymer backbone affect the interaction with water in different cellulose derivatives, which will dictate the carrier properties when applied in a solid dispersion.

### **4.2.1 Structure formation in extrusion processing**

In paper I the effect from the processing method, hot melt extrusion, for the formation of structures and orientations in a dispersion of carbamazepine in ethyl cellulose was examined using PXCT and scanning SAXS/WAXS. In the hot melt extrusion, the components of drug and carrier are fed into a heated barrel containing two co-rotating screws. The exposure to the heat from the barrel and the shear stress from the rotating screws melt the material and mix and convey the two components until finally ejected through a die<sup>27</sup>. Figure 4.3 shows a schematic over the extrusion process and the results for the orientational analysis of the sample from scanning SAXS and the directly resolved morphology from PXCT. Scanning SAXS measurements were made over the bulk filament, parallel to the direction of extrusion and over a cross section of the sample, perpendicular to the direction of extrusion. The measurement over the bulk filament shows that the sample is ordered in the direction of extrusion while the measurement over the cross section shows a circular orientation around the centre of the filament, which is stronger towards the edge of the filament while in the centre the scattering is nearly isotropic. With PXCT the orientation of drug domains is directly resolved in a sub volume of 50\*50\*15  $\mu\text{m}$ , extracted from the centre of the filament. Here the

domains also show a strong orientation along the direction of extrusion as well as a spiral orientation in the centre of the filament. This spiral orientation is not detected in the SAXS experiment which is explained by the statistical nature of the method, measuring an average of all orientations along the thickness of the sample, leading to nearly isotropic scattering in the centre of the filament due to multiple orientations along the thickness of the sample. The combination of these two results reveals that there is a high orientation in the entire filament as a consequence of the extrusion processing. This suggests that the phase separation of the drug domains is present already in the extrusion process and that the high drug concentration hinders the carbamazepine from being fully dispersed in the ethyl cellulose matrix. When the sample is extruded and cooled down to room temperature it passes the glass transition temperature of the mixture that locks in the structure and the induced orientation will remain, indicating that the morphology is created as a consequence of the high-shear extrusion process. The stronger anisotropy observed in the edge of the filament in the SAXS experiment suggests that there is a shear gradient in the extrusion process from the walls of the die, resulting in a strong alignment towards the edge of the filament.

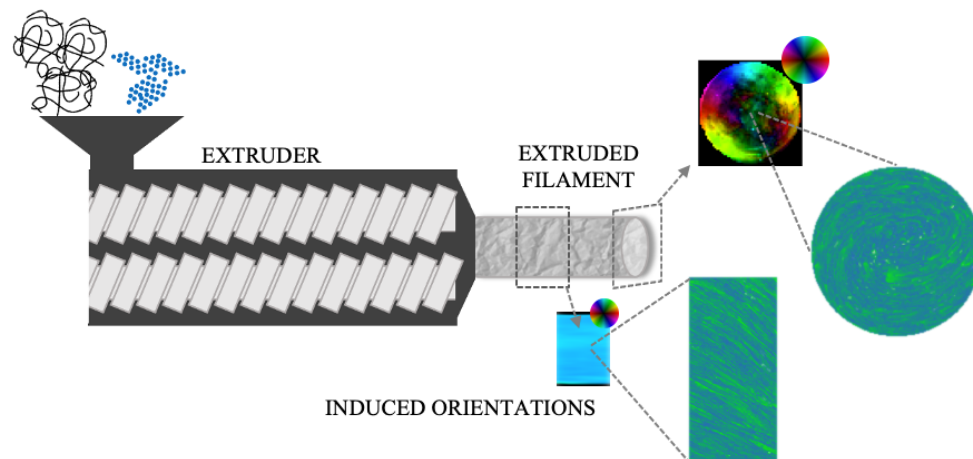


**Figure 4.3.** Schematic over structures formed during extrusion.

#### **4.2.2 Morphologies relation to composition and release rate in phase separated dispersions**

In paper II, the morphology of dispersions with a phase separated polymer carrier was investigated using PXCT and STXM. The purpose of the phase separated morphology is to create formulations with controlled drug release, where the morphology dictates the release rate. For this, nicotinamide was dispersed in a mixture of hydrophilic HPMC and hydrophobic PLA, with the intention of HPMC to work as a channelling agent through the insoluble PLA, creating a porous network upon dissolution. To enable a tailoring of the drug dissolution profile, an understanding of both the connection between the formation of the morphology as a result of composition and processing and how the morphology affects the dissolution characteristics needs to be established.

To understand the relation between the morphology and the drug concentration, dispersions with different nicotinamide concentrations were measured with PXCT. Figure 4.4 shows 2D slices extracted from the reconstructed 3D volumes of dispersions with 0-30wt% nicotinamide in 70/30 PLA/HPMC. In the dispersion with 10wt% nicotinamide, the drug is amorphous and dispersed in both polymer phases, as confirmed with WAXS and STXM. PLA has a higher electron density ( $0.405 \text{ e}/\text{\AA}^3$ ) than HPMC ( $0.399 \text{ e}/\text{\AA}^3$ ) thus PLA-rich domains shows up as bright domains in Figure 4.4a-b. However, in the dispersion with 30wt% nicotinamide, the drug has partly crystallised which increase the electron density in the system. The bright phase here in Fig 4c, corresponds to regions with crystallised nicotinamide which can be seen occupy a large fraction of the HPMC rich phase and appear as small crystallites in the PLA matrix.

The solid dispersion of 70/30 PLA/HPMC ratio without nicotinamide, Figure 4.4a, shows that the HPMC phase is mainly distributed as smaller isolated microdomains in the PLA matrix, although larger HPMC domains also exist. With addition of drug, Figure 4.4b, the HPMC domains grow and the connectivity of the HPMC domains increases. At the highest drug concentration, Figure 4.4c, the HPMC rich domains are more spherical and isolated and dominated by crystallised nicotinamide. The spherical domains have an internal swirling pattern of HPMC rich and nicotinamide rich regions. The change in morphology as a function of drug concentration can be attributed to the plasticising effect of the nicotinamide which increases the molecular mobility and lowers the viscosity of the polymer blend during the extrusion process. At first, this allows for the formation of larger, more connected domains, however, with an increased drug load the low melt viscosity instead leads to formation of disconnected, drop like spheres.

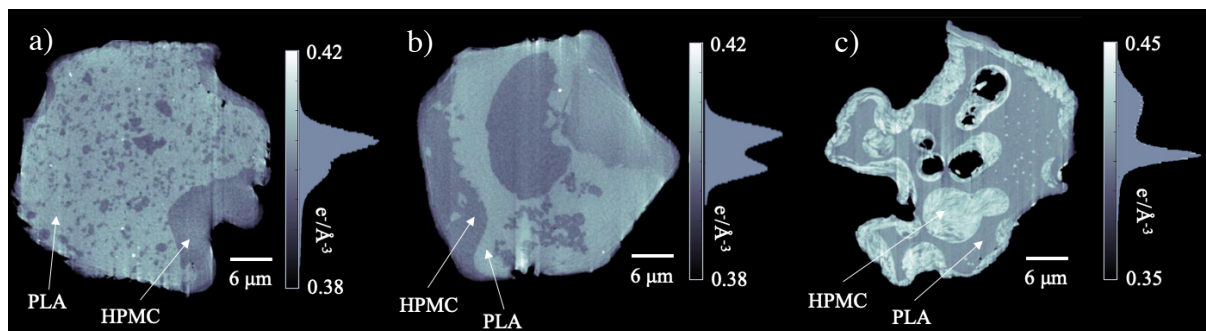


**Figure 4.4.** PXCT results showing a change in morphology depending on drug concentration in the dispersion. Tomography slices extracted from reconstructed 3D volumes of a) 0wt% b) 10wt% and c) 30wt% Nicotinamide in 70/30 PLA/HPMC. Due to the increased electron density in the sample with crystallised nicotinamide the colour scale is shifted in c).

To understand the relation between the morphology and the polymer fraction, dispersions with different PLA/HPMC ratio and fixed drug concentration were compared. Figure 4.5 show 2D slices extracted from the reconstructed 3D volumes and the corresponding 3D reconstructions of the segmented HPMC domains. The dispersion with polymer fraction 50/50 PLA/HPMC shows a morphology with aggregated domains of HPMC with size of a few  $\mu\text{m}$  that together build up a connected network over the sample volume. The dispersion with 70/30 PLA/HPMC shows a morphology with both small HPMC domains, just below 1

$\mu\text{m}$ , and larger domains that span almost the entire size of the 2D slice. However, the domains are still connected within the 3D morphology as illustrated in Figure 4.5d, with smaller more tortuous HPMC domains that connects the larger domains. Comparing the two morphologies the connectivity of HPMC domains increases in the dispersion with higher HPMC content. This can simply be attributed to the higher fraction of HPMC.

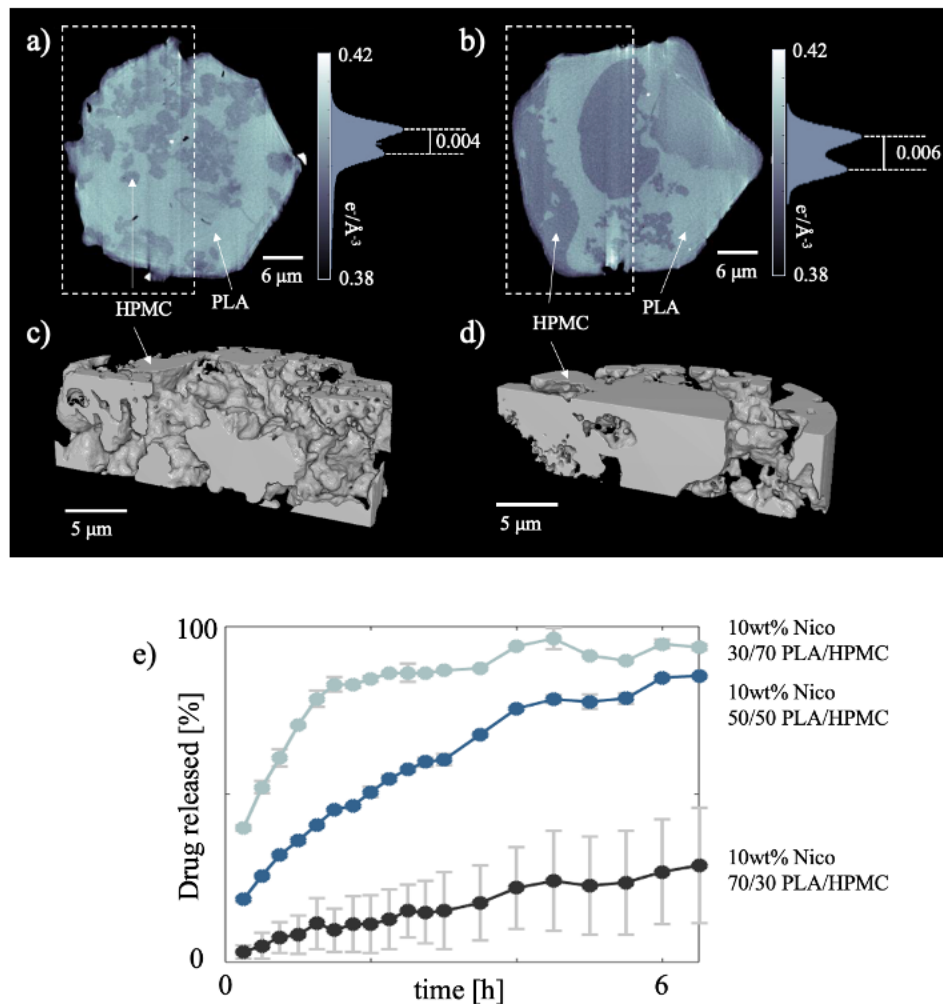


**Figure 4.5.** Tomography slices extracted from the reconstructed 3D volumes of 10wt% nicotinamide in 50/50 PLA/HPMC and b) 70/30 PLA/HPMC with c-d) 3D volume renderings of the segmented HPMC rich domains in respective dispersions and e) release profiles of the phase separated dispersions of varying polymer composition.

The morphologies of the dispersions can be related to the dissolution characteristics, Figure 4.5e. Both the dispersions with 50/50 and 70/30 PLA/HPMC fraction shows extended-release profiles. In the dispersion with 50/50 PLA/HPMC fraction, the dissolution curve shows a fast initial release that transitions to a linear shape after the first hour. After 6 hours, 80% of the total expected drug content in the dispersion is released. At lower HPMC content, 70/30 PLA/HPMC, a linear release rate is observed and only 20% of the total expected drug content is released after the 6 h. The nicotinamide is dispersed in both phases at a comparable concentration, thus, also drug in the insoluble PLA matrix has been released from the 50/50 PLA/HPMC dispersion, where 80% of the total drug fraction is released. A suggested

explanation to this can be the swelling of the HPMC phase during dissolution, causing a distortion of the PLA phase. The distortion of the PLA phase will expose a larger area of the PLA matrix to the dissolution media and decrease diffusion paths, enabling release of nicotinamide also from the insoluble matrix. The extended release is expected to be a result of the phase separated morphology where the channels created by the HPMC phase in the PLA matrix create a network that decreases the rate of nicotinamide molecules to reach the release media. In the dispersion of 10wt% nicotinamide in 70/30 PLA/HPMC the lower fraction of HPMC will lead to a lesser connectivity of HPMC domains and less swelling of the structure, and more nicotinamide is trapped in the interior of the insoluble matrix resulting in a low total expected drug release of 20% after 6h.

### **4.2.3 Relations between properties and molecular structure**

Cellulose-based solid dispersions will be affected by the environment it is exposed to both during storage and dissolution. The chosen polymer carrier will largely influence this depending on its hydrophilicity and dissolution characteristics. In paper III we investigated how the structure of substituted side chains in modified cellulose is related to the thermal properties and water absorption of the cellulose derivative. To do this, cellulose acetate (CA) and cellulose acetate butyrate (CAB), with similar total degree of substitution, but different length of substituted side chains, were melt pressed to films and left at in air respectively soaked in water for 72 h. CA are substituted with shorter acetate groups while CAB is substituted by a mixture of cellulose acetate groups and longer butyrate groups. The different grades of CAB are referred to as CAB I, II and III with increasing ratio of longer butyrate chains. Figure 4.6a shows the WAXS results of unconditioned, and wet conditioned films together with the measured water absorption and the degree of substitution of acetate,  $DS_A$ , and butyrate,  $DS_B$ . Films of CA and CAB I are semicrystalline, as observed by the sharp peaks in the scattering curve while CAB II and CAB III are amorphous, as observed by the broad amorphous peaks and lack of sharp crystalline peaks. This shows that longer side chains decrease the crystallinity, which can be related to the effect of disrupting the ordering of cellulose in the crystalline lattice. The water exposure causes two main differences. For films with high water absorption, an increased intensity at high  $q$  is observed, as marked in Figure 4.6a, and attributed to a contribution of the absorbed water to the WAXS signal. In CA and CAB I, the exposure to water also results in more prominent peaks, indicating an increase in local packing patterns and slight increase in crystallinity. CAB II and CAB III only show minor changes which agrees with the low amount of water absorbed. The changes in the scattering pattern from the films are more pronounced for cellulose derivatives substituted with shorter chains. This is related to a screening effect by longer side chains hindering water penetration in the cellulose structure and reducing the ability for hydrogen bonding with the hydroxyl groups on the cellulose backbone, as illustrated in Figure 4.6b. Here this is studied for homogenous cellulose derivatives, but similar mechanisms can be used for tailoring properties of a solid dispersions with adapting the selected cellulose carrier.

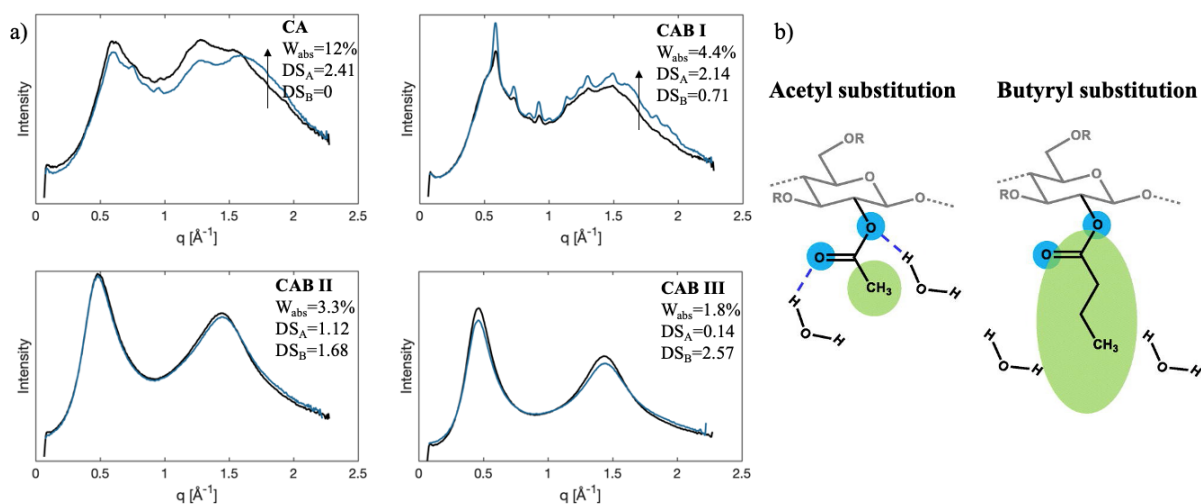


**Figure 4.6.** a) WAXS curves for melt pressed films unconditioned (black) and wet conditioned films (blue) for cellulose acetate and cellulose acetate butyrate with different ratio of butyrate substituents. b) Schematic over the screening of hydrogen bonds with increased substituent chain length.

### 4.3 Addressing radiation damage

Radiation damage pose a challenge for applying PXCT and STXM to cellulose-based solid dispersions. The exposure to ionizing radiation may lead to structural changes and therefore it is important to both limit the radiation dose and confirm that the analysed structures are native to the sample and not formed by beam exposure. For this purpose, radiation damage should be investigated where the sample is exposed to an accumulated level of radiation dose where structural changes start to appear. This dose can then be used as a threshold value for what level of radiation is safe to expose the sample to.

In paper I and II PXCT measurements are performed under cryogenic conditions by using the specific OMNY setup available at the cSAXS beamline<sup>46</sup>. However, keeping the sample at cryogenic conditions does not hinder radiation damage, but rather keeps the structure intact during the measurement as shown by Beetz and Jacobsen<sup>62</sup> that demonstrated that the C=O bond breaking in a PMMA sample were similar both under cryogenic conditions and room temperature while the mass loss was distinctively reduced under cryogenic conditions. This works well for the PXCT measurements where inhomogeneities in electron density in the sample is the contrast agent but is less efficient for STXM where the bonding structure is analysed and used as contrast mechanism in the imaging.

To confirm that the structures are kept intact during the PXCT measurement, each tomogram is divided into two sub-tomograms, reconstructed independently from the first and second half of the projections respectively. If structure in the dispersions would evolve due to beam damage, this would be discovered by a change between the two sub-tomograms. Figure 4.7 shows this evaluation for the carbamazepine dispersion investigated in paper I. The small subareas of the full tomogram and the two sub-tomograms shows similar patterns, demonstrating the absence of structural change during the measurement, confirming that the sample is exposed to an acceptable dose level.

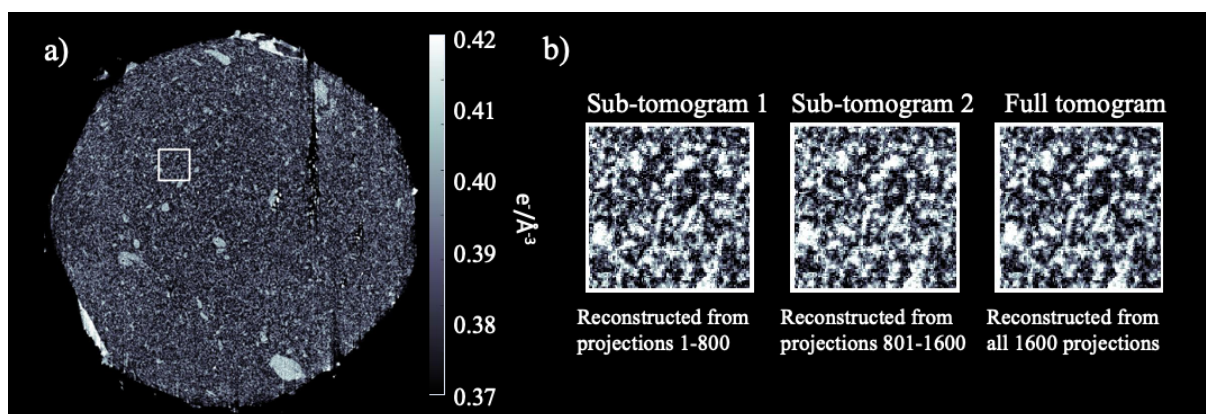


**Figure 4.7.** a) Full tomogram of the carbamazepine dispersion from paper I b) Zoomed in regions in Sub-tomograms reconstructed from two individually sampled sets of the first 800 and last 800 projections of the full tomogram. The absence of structural change indicates that the structure kept intact during the measurement and that a controllable level of radiation dose is impinged on the sample.

For the STXM measurements an optimized measuring protocol were utilized for limiting radiation damage effects. Figure 4.8 shows spectra that are subsequently acquired the same line over a PLA rich region in one of the dispersions in paper II with an accumulated exposure time of 5ms and 20ms, respectively. The spectrum of the dispersion keeps intact over the radiation dose accumulated by 4 x 5ms, however with repeated measurements of 20ms both mass losses, as seen by the decreased optical density in the spectra, as well as chemical changes from a decrease in the resonance peak at 288.0 eV from the  $C\ 1s \rightarrow 1\pi^*_{(C=O)}$  transition in PLA and the appearance of a peak at 286.1 eV are observed. This indicates that a dwell time of 20ms for a single measurement with high spectral resolution is regarded as a safe dose level but with repeated measurements the sample will start to degrade.

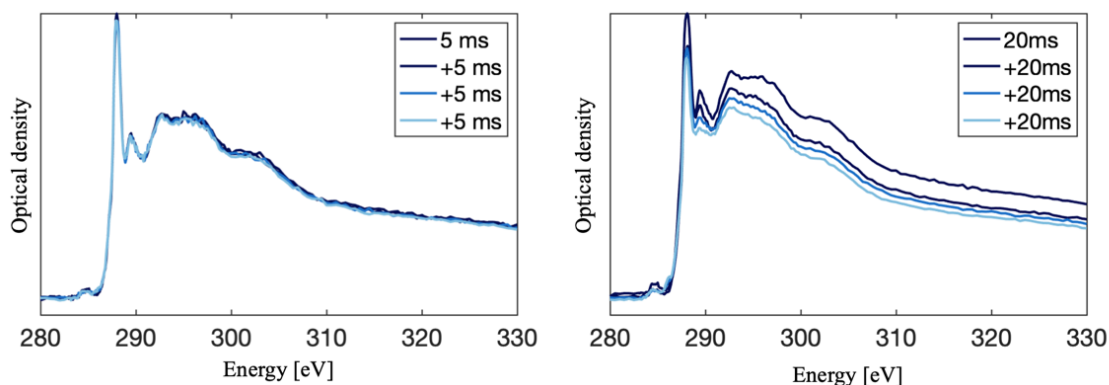


**Figure 4.8.** NEXAFS spectra measured by repeated measurements over the same PLA rich region in a dispersion from paper II with a) 5 ms dwell time and b) 20 ms dwell time. The spectra with the short dwell time of 5ms remains intact over the subsequent measurements while the longer dwell time of 20 ms show large changes between subsequent measurements.

Apart from adapting the exposure time, measurements can also be optimised for limiting radiation damage and circumvent the need for compromising between spectral and spatial resolution and decreased statistics from decreased exposure times. This can be done by optimising for different criteria in different regions of the spectra. When a spectrum is collected for evaluating the qualitative analysis, a high spectral resolution with good statistics

is desired but the spatial resolution is less important. Then the exposure time in each measurement can be decreased, the beam defocused and an average of the signal over a larger region can be used for building up the high-quality spectrum. When a high spatial resolution is needed, a few energies corresponding to the resonances of the materials of interest can be selected and for increasing the statistics the exposure time in each point can be increased, as much fewer energies are collected, which leads to less averaging needed for a good signal and images of high resolution can be acquired.



# Chapter 5 - Conclusions and Outlook

This thesis presents PXCT, scanning SAXS/WAXS and, STXM with NEXAFS contrast as unique methods for multiscale and multimodal imaging of solid dispersions. The use of correlative X-ray techniques for multiscale imaging with different contrast mechanisms provides a basis for understanding connections between the formation of structures and their relation to functional properties of the formulation. The combination of PXCT and scanning SAXS/WAXS presents an imaging approach where the directly resolved morphology from PXCT can be correlated to the statistical representation of nanostructures mapped over a macroscopic bulk sample with scanning SAXS/WAXS, while simultaneously characterising the solid-state phase of the material from the sample scattering. In practise, for cellulose dispersions, this means that the nano and microstructures formed from for instance drug aggregation, phase separation or porosities can be imaged directly, non-destructively, with a resolution of sub-100 nm with a field of view of tens of micrometres. To further understand how these morphologies extend over a full tablet, film or extruded filament, the nano structural information gained from the scattering of the sample can be mapped with a resolution similar to the volume imaged in the nanotomography. This also allow for a correlation between the scattering signal and the imaged morphology, simplifying the interpretation of the statistical structural information. Simultaneously, the solid-phase and molecular arrangement of the sample is mapped, allowing for a better understanding of the different components by determining if the sample is crystalline or amorphous, if the components are homogenously mixed over the sample and also allows for characterising and distinguish between different drug polymorphs.

Another approach is to combine STXM with NEXAFS contrast and the scattering-based techniques such as PXCT. STXM with NEXAFS has a unique capability for characterising the chemical content and determine compositional changes in the phase such as determining if samples are fully phase separated and spatially map the drug partitioning. Due to high sensitivity to small chemical changes such as substituted moieties this technique can also be useful for studying chemical modifications in cellulose derivatives and both spatially map and quantify modifications in cellulose materials.

A future direction for the methodologies presented in this work is the possibility for imaging with high temporal resolution. This presents a possibility for also studying how the morphology changes during different processes. For instance, X-ray microcomputed tomography can be useful for characterising changes in the morphology during dissolution of solid dispersions and scattering experiments can be used for studying how structures evolve during cooling of an extruded strand or during solvent evaporation or dissolution to better understand the formation and evolvment of these structures in solid dispersions.

With the advances of both lab scale and synchrotron X-ray techniques the sensitivity, spatial resolution and possibilities for multimodal imaging will continue to improve. However, for cellulose-based solid dispersions to be able to take advantage of these unique characterisation

methods issues with radiation damage needs to be addressed and a proper understanding of the risks for structural changes from X-ray beam interaction needs to be developed. With that fulfilled, X-ray analysis has great prospects to continue to provide novel insights for how morphologies and structural properties of pharmaceutical formulations affect the materials and how this can be used to tailor properties for the development of new formulations and drug delivery systems.

# Acknowledgements

First and foremost, I would like to thank my supervisors, Aleksandar Matic and Marianne Liebi. I cannot think of a better team, and I feel spoiled with having two such amazing supervisors! Thank you, Aleksandar, for being so enthusiastic and always dedicating time for discussions. Thank you, Marianne, for being so supportive and positive for new ideas and projects.

A big thanks to all members of the Liebi group and Matic group for all the discussions collaborations and fun times! A special thanks to Linnea Björn for the many late hours together at various beamtimes, I would never have survived 11 days of STXM beamtime without you! Also to Christian Appel for always having time for discussions and sharing your knowledge, which sometimes makes me wonder if there is something that you do not know. Thanks to all of the Materials Physics division for being so welcoming and helpful.

I would also like to thank all my collaborators and co-authors. A special thanks to Robin Nilsson, Rydviha Govender and Anette Larsson for lending me your materials for performing various experiments! I really enjoy working with you and all our discussions taught me a lot in the world of pharmaceuticals.

I also acknowledge the Excellence Initiative Nano at Chalmers for funding this work and the EUSMI program and the Paul Scherrer Institute for granting access to synchrotron radiation beamtime at the cSAXS and PoLux beamlines at the Swiss Light source. Thanks to the cSAXS and PoLUX team, especially Ana Diaz, Mirko Holler, and Benjamin Watts for bringing your expertise and always being so involved and dedicated in making the best possible experiment!

Finally, thanks to my family and friends for always cheering me on. You are the best, my source of motivation and biggest supporters!



# Bibliography

1. Ventura-Cruz, S.; Tecante, A., Nanocellulose and microcrystalline cellulose from agricultural waste: Review on isolation and application as reinforcement in polymeric matrices. *Food Hydrocolloids* **2021**, *118*, 106771.
2. Yu, L., *Biodegradable polymer blends and composites from renewable resources*. John Wiley & Sons: 2009.
3. Chavan, R. B.; Rathi, S.; Jyothi, V. G. S.; Shastri, N. R., Cellulose based polymers in development of amorphous solid dispersions. *Asian journal of pharmaceutical sciences* **2019**, *14* (3), 248-264.
4. Klemm, D.; Heublein, B.; Fink, H. P.; Bohn, A., Cellulose: fascinating biopolymer and sustainable raw material. *Angewandte chemie international edition* **2005**, *44* (22), 3358-3393.
5. Shokri, J.; Adibkia, K., Application of cellulose and cellulose derivatives in pharmaceutical industries. In *Cellulose-medical, pharmaceutical and electronic applications*, IntechOpen: 2013.
6. Sershen, S.; West, J., Implantable, polymeric systems for modulated drug delivery. *Advanced drug delivery reviews* **2002**, *54* (9), 1225-1235.
7. Tran, P. H.-L.; Tran, T. T.-D.; Park, J. B.; Lee, B.-J., Controlled release systems containing solid dispersions: strategies and mechanisms. *Pharmaceutical research* **2011**, *28* (10), 2353-2378.
8. Baghel, S.; Cathcart, H.; O'Reilly, N. J., Polymeric Amorphous Solid Dispersions: A Review of Amorphization, Crystallization, Stabilization, Solid-State Characterization, and Aqueous Solubilization of Biopharmaceutical Classification System Class II Drugs. *J Pharm Sci* **2016**, *105* (9), 2527-2544.
9. Ricarte, R. G.; Van Zee, N. J.; Li, Z.; Johnson, L. M.; Lodge, T. P.; Hillmyer, M. A., Recent Advances in Understanding the Micro- and Nanoscale Phenomena of Amorphous Solid Dispersions. *Mol Pharm* **2019**, *16* (10), 4089-4103.
10. Hallouard, F.; Mehenni, L.; Lahiani-Skiba, M.; Anouar, Y.; Skiba, M., Solid Dispersions for Oral Administration: An Overview of the Methods for their Preparation. *Curr Pharm Des* **2016**, *22* (32), 4942-4958.
11. Nie, H.; Xu, W.; Taylor, L. S.; Marsac, P. J.; Byrn, S. R., Crystalline solid dispersion- a strategy to slowdown salt disproportionation in solid state formulations during storage and wet granulation. *International Journal of Pharmaceutics* **2017**, *517* (1-2), 203-215.
12. Sanabria Ortiz, K.; Hernández Espinell, J. R.; Ortiz Torres, D.; Lopez-Mejias, V.; Stelzer, T., Polymorphism in solid dispersions. *Crystal Growth & Design* **2019**, *20* (2), 713-722.

13. Willmott, P., *An introduction to synchrotron radiation: techniques and applications*. John Wiley & Sons: 2019.
14. Baird, J. A.; Taylor, L. S., Evaluation of amorphous solid dispersion properties using thermal analysis techniques. *Adv Drug Deliv Rev* **2012**, *64* (5), 396-421.
15. Lipinski, C. A.; Lombardo, F.; Dominy, B. W.; Feeney, P. J., Experimental and computational approaches to estimate solubility and permeability in drug discovery and development settings. *Advanced drug delivery reviews* **1997**, *23* (1-3), 3-25.
16. Van den Mooter, G., The use of amorphous solid dispersions: A formulation strategy to overcome poor solubility and dissolution rate. *Drug Discovery Today: Technologies* **2012**, *9* (2), e79-e85.
17. Schittny, A.; Huwyler, J.; Puchkov, M., Mechanisms of increased bioavailability through amorphous solid dispersions: a review. *Drug Delivery* **2020**, *27* (1), 110-127.
18. Bhujbal, S. V.; Mitra, B.; Jain, U.; Gong, Y.; Agrawal, A.; Karki, S.; Taylor, L. S.; Kumar, S.; Zhou, Q. T., Pharmaceutical amorphous solid dispersion: A review of manufacturing strategies. *Acta Pharmaceutica Sinica B* **2021**, *11* (8), 2505-2536.
19. Vo, C. L.-N.; Park, C.; Lee, B.-J., Current trends and future perspectives of solid dispersions containing poorly water-soluble drugs. *European journal of pharmaceuticals and biopharmaceutics* **2013**, *85* (3), 799-813.
20. Zhang, M.; Li, H.; Lang, B.; O'Donnell, K.; Zhang, H.; Wang, Z.; Dong, Y.; Wu, C.; Williams III, R. O., Formulation and delivery of improved amorphous fenofibrate solid dispersions prepared by thin film freezing. *European journal of pharmaceuticals and biopharmaceutics* **2012**, *82* (3), 534-544.
21. Chavan, R. B.; Rathi, S.; Jyothi, V.; Shastri, N. R., Cellulose based polymers in development of amorphous solid dispersions. *Asian J Pharm Sci* **2019**, *14* (3), 248-264.
22. Wasilewska, K.; Winnicka, K., Ethylcellulose—a pharmaceutical excipient with multidirectional application in drug dosage forms development. *Materials* **2019**, *12* (20), 3386.
23. Maggi, L.; Machiste, E. O.; Torre, M. L.; Conte, U., Formulation of biphasic release tablets containing slightly soluble drugs. *European journal of pharmaceuticals and biopharmaceutics* **1999**, *48* (1), 37-42.
24. Velasco, M. V.; Ford, J. L.; Rowe, P.; Rajabi-Siahboomi, A. R., Influence of drug: hydroxypropylmethylcellulose ratio, drug and polymer particle size and compression force on the release of diclofenac sodium from HPMC tablets. *Journal of Controlled Release* **1999**, *57* (1), 75-85.
25. Vargas, C. I.; Ghaly, E. S., Kinetic release of theophylline from hydrophilic swellable matrices. *Drug development and industrial pharmacy* **1999**, *25* (9), 1045-1050.
26. Maniruzzaman, M.; Boateng, J. S.; Snowden, M. J.; Douroumis, D., A review of hot-melt extrusion: process technology to pharmaceutical products. *ISRN Pharm* **2012**, *2012*, 436763.

27. LaFontaine, J. S.; McGinity, J. W.; Williams, R. O., Challenges and strategies in thermal processing of amorphous solid dispersions: a review. *Aaps Pharmscitech* **2016**, *17* (1), 43-55.
28. Brazel, C. S.; Peppas, N. A., Modeling of drug release from swellable polymers. *European journal of pharmaceuticals and biopharmaceutics* **2000**, *49* (1), 47-58.
29. Ehtezazi, T.; Washington, C., Controlled release of macromolecules from PLA microspheres: using porous structure topology. *Journal of controlled release* **2000**, *68* (3), 361-372.
30. Gillespie, A. W.; Phillips, C. L.; Dynes, J. J.; Chevrier, D.; Regier, T. Z.; Peak, D., Advances in using soft X-ray spectroscopy for measurement of soil biogeochemical processes. *Advances in agronomy* **2015**, *133*, 1-32.
31. Withers, P. J., X-ray nanotomography. *Materials today* **2007**, *10* (12), 26-34.
32. Schnablegger, H.; Singh, Y., The SAXS guide. Getting acquainted with the principles (Anton Paar GmbH). **2013**.
33. Bunk, O.; Bech, M.; Jensen, T.; Feidenhans, R.; Binderup, T.; Menzel, A.; Pfeiffer, F., Multimodal x-ray scatter imaging. *New Journal of Physics* **2009**, *11* (12), 123016.
34. Wu, H.; Chen, R.; Li, Z., Optimization of sample thickness for small angle X-ray scattering (SAXS). *Instrumentation Science & Technology* **2022**, 1-15.
35. Pauw, B. R., Everything SAXS: small-angle scattering pattern collection and correction. *Journal of Physics: Condensed Matter* **2013**, *25* (38), 383201.
36. Dierolf, M.; Menzel, A.; Thibault, P.; Schneider, P.; Kewish, C. M.; Wepf, R.; Bunk, O.; Pfeiffer, F., Ptychographic X-ray computed tomography at the nanoscale. *Nature* **2010**, *467* (7314), 436-9.
37. Baruchel, J.; Buffiere, J.-Y.; Maire, E., X-ray tomography in material science. **2000**.
38. Schofield, R.; King, L.; Tayal, U.; Castellano, I.; Stirrup, J.; Pontana, F.; Earls, J.; Nicol, E., Image reconstruction: Part 1 - understanding filtered back projection, noise and image acquisition. *J Cardiovasc Comput Tomogr* **2020**, *14* (3), 219-225.
39. Liu, Y.; Nelson, J.; Holzner, C.; Andrews, J.; Pianetta, P., Recent advances in synchrotron-based hard x-ray phase contrast imaging. *Journal of Physics D: Applied Physics* **2013**, *46* (49), 494001.
40. Pfeiffer, F., X-ray ptychography. *Nature Photonics* **2018**, *12* (1), 9-17.
41. Thibault, P.; Guizar-Sicairos, M.; Menzel, A., Coherent imaging at the diffraction limit. *Journal of synchrotron radiation* **2014**, *21* (5), 1011-1018.
42. Diaz, A.; Trtik, P.; Guizar-Sicairos, M.; Menzel, A.; Thibault, P.; Bunk, O., Quantitative x-ray phase nanotomography. *Physical Review B* **2012**, *85* (2), 020104.

43. Holler, M.; Diaz, A.; Guizar-Sicairos, M.; Karvinen, P.; Färm, E.; Härkönen, E.; Ritala, M.; Menzel, A.; Raabe, J.; Bunk, O., X-ray ptychographic computed tomography at 16 nm isotropic 3D resolution. *Scientific reports* **2014**, *4* (1), 1-5.
44. Holler, M.; Ihli, J.; Tsai, E. H. R.; Nudelman, F.; Verezhak, M.; van de Berg, W. D. J.; Shahmoradian, S. H., A lathe system for micrometre-sized cylindrical sample preparation at room and cryogenic temperatures. *J Synchrotron Radiat* **2020**, *27* (Pt 2), 472-476.
45. Yuan, H.; Yuan, H.; Casagrande, T.; Shapiro, D.; Yu, Y.-S.; Enders, B.; Lee, J. R.; van Buuren, A.; Biener, M. M.; Gammon, S. A., 4D Imaging of ZnO-Coated Nanoporous Al<sub>2</sub>O<sub>3</sub> Aerogels by Chemically Sensitive Ptychographic Tomography: Implications for Designer Catalysts. *ACS Applied Nano Materials* **2021**, *4* (1), 621-632.
46. Holler, M.; Raabe, J.; Diaz, A.; Guizar-Sicairos, M.; Wepf, R.; Odstreil, M.; Shaik, F. R.; Panneels, V.; Menzel, A.; Sarafimov, B.; Maag, S.; Wang, X.; Thominet, V.; Walther, H.; Lachat, T.; Vitins, M.; Bunk, O., OMNY-A tOMography Nano crYo stage. *Rev Sci Instrum* **2018**, *89* (4), 043706.
47. Guizar-Sicairos, M.; Boon, J. J.; Mader, K.; Diaz, A.; Menzel, A.; Bunk, O., Quantitative interior x-ray nanotomography by a hybrid imaging technique. *Optica* **2015**, *2* (3).
48. Guizar-Sicairos, M.; Diaz, A.; Holler, M.; Lucas, M. S.; Menzel, A.; Wepf, R. A.; Bunk, O., Phase tomography from x-ray coherent diffractive imaging projections. *Optics express* **2011**, *19* (22), 21345-21357.
49. Thibault, P.; Dierolf, M.; Bunk, O.; Menzel, A.; Pfeiffer, F., Probe retrieval in ptychographic coherent diffractive imaging. *Ultramicroscopy* **2009**, *109* (4), 338-43.
50. van Heel, M.; Schatz, M., Fourier shell correlation threshold criteria. *J Struct Biol* **2005**, *151* (3), 250-62.
51. Hitchcock, A. P., Soft X-ray spectromicroscopy of polymers and biopolymer interfaces. *Journal of synchrotron radiation* **2001**, *8* (2), 66-71.
52. Yu, Y.-S.; Farmand, M.; Kim, C.; Liu, Y.; Grey, C. P.; Strobridge, F. C.; Tyliczszak, T.; Celestre, R.; Denes, P.; Joseph, J., Three-dimensional localization of nanoscale battery reactions using soft X-ray tomography. *Nature communications* **2018**, *9* (1), 1-7.
53. Hähner, G., Near edge X-ray absorption fine structure spectroscopy as a tool to probe electronic and structural properties of thin organic films and liquids. *Chemical Society Reviews* **2006**, *35* (12), 1244-1255.
54. Stöhr, J., *NEXAFS spectroscopy*. Springer Science & Business Media: 1992; Vol. 25.
55. Urquhart, S. G.; Hitchcock, A. P.; Smith, A. P.; Ade, H. W.; Lidy, W.; Rightor, E. G.; Mitchell, G. E., NEXAFS spectromicroscopy of polymers: overview and quantitative analysis of polyurethane polymers. *Journal of Electron Spectroscopy and Related Phenomena* **1999**, *100* (1-3), 119-135.
56. Koprinarov, I.; Hitchcock, A.; McCrory, C.; Childs, R., Quantitative mapping of structured polymeric systems using singular value decomposition analysis of soft X-ray images. *The Journal of Physical Chemistry B* **2002**, *106* (21), 5358-5364.

57. Holton, J. M., A beginner's guide to radiation damage. *Journal of synchrotron radiation* **2009**, *16* (2), 133-142.
58. Meents, A.; Gutmann, S.; Wagner, A.; Schulze-Briese, C., Origin and temperature dependence of radiation damage in biological samples at cryogenic temperatures. *Proceedings of the National Academy of Sciences* **2010**, *107* (3), 1094-1099.
59. Hettel, R., DLSR design and plans: an international overview. *Journal of synchrotron radiation* **2014**, *21* (5), 843-855.
60. Gianoncelli, A.; Vaccari, L.; Kourousias, G.; Cassese, D.; Bedolla, D.; Kenig, S.; Storici, P.; Lazzarino, M.; Kiskinova, M., Soft X-ray microscopy radiation damage on fixed cells investigated with synchrotron radiation FTIR microscopy. *Scientific reports* **2015**, *5* (1), 1-11.
61. Howells, M. R.; Beetz, T.; Chapman, H. N.; Cui, C.; Holton, J.; Jacobsen, C.; Kirz, J.; Lima, E.; Marchesini, S.; Miao, H., An assessment of the resolution limitation due to radiation-damage in x-ray diffraction microscopy. *Journal of electron spectroscopy and related phenomena* **2009**, *170* (1-3), 4-12.
62. Beetz, T.; Jacobsen, C., Soft X-ray radiation-damage studies in PMMA using a cryo-STXM. *Journal of synchrotron radiation* **2003**, *10* (3), 280-283.

